Journal of Photochemistry and Photobiology A: Chemistry 234 (2012) 135–145

Contents lists available at SciVerse ScienceDirect

Journal of Photochemistry and Photobiology A: Chemistry

journal homepage: www.elsevier.com/locate/jphotochem

Photoantenna in two cryptochrome–photolyase proteins from *O. tauri*: Presence, nature and ultrafast photoinduced dynamics

Johanna Brazard[a], Christian Ley[a], Fabien Lacombat[a], Pascal Plaza[a,*], Laetitia Mony[b], Marc Heijde[c], Gérald Zabulon[c], Chris Bowler[c]

[a] *UMR 8640 CNRS-ENS-UPMC, Département de Chimie, École Normale Supérieure, 24 rue Lhomond, 75005 Paris, France*
[b] *UMR 8601 CNRS, Laboratoire de Chimie et Biochimie Pharmacologies et Toxicologiques, Université Paris Descartes, 12 rue de l'École de médecine, 75006 Paris, France*
[c] *UMR 8186 CNRS-ENS, Département de Biologie, École Normale Supérieure, 46 rue d'Ulm, 75005 Paris, France*

ARTICLE INFO

Article history:
Available online 31 January 2012

Keywords:
Photoantenna
MTHF
8-HDF
Cryptochrome
Photolyase
Ultrafast spectroscopy
Transient absorption
Femtosecond

ABSTRACT

Cryptochromes and photolyases are homologous flavoproteins either involved in photosensory functions or in the photorepair of UV-damaged DNA. We report on the presence, nature and ultrafast photoinduced dynamics of a photoantenna in two recently discovered cryptochrome/photolyase proteins (OtCPF1, a (6-4) photolyase, and OtCPF2, a cryptochrome-DASH), coming from the green alga *Ostreococcus tauri*. Whereas OtCPF1 does not show any apparent photoantenna after purification, OtCPF2 is found to bind the folate MTHF. Resonance energy transfer, from MTHF to the flavin cofactor (FAD) of OtCPF2, was studied by femtosecond transient absorption spectroscopy. It takes place in 15 ps when FAD is oxidized and 100 ps when it is fully reduced. The intrinsic photophysics of MTHF in acidic solution was studied for comparison. Two decays in the sub-100 ps regime were tentatively attributed to the presence of two conformers or to a quenching mechanism involving large-amplitude motions of the 1,2,3,4-tetrahydropyraxine ring. On the other hand, the nature of the missing photoantenna of OtCFP1 was questioned by means of sequence alignment and homology modeling. We propose that the deazaflavin 8-HDF could be the photoantenna of OtCFP1 *in vivo*.

1. Introduction

Cryptochromes and photolyases form a family (called CPF) of homologous flavoproteins involved in different light-activated biological functions [1]. Photolyases are able to photorepair UV-damaged DNA without nucleotide excision: CPD photolyases split cyclobutane pyrimidine dimers [1–3], and (6-4) photolyases repair the pyrimidine (6-4) pyrimidone photoproducts [1]. Cryptochromes are signaling photoreceptors [1,4–8], but cryptochromes-DASH are believed to exhibit specialized single-stranded photolyase activity [9,10]. All CPF proteins non-covalently bind flavin adenine dinucleotide (FAD, Fig. 1, left) as the main photoactive cofactor. They generally bind a secondary cofactor, a photoantenna that absorbs light with large extinction coefficient and improves the efficiency of the protein through resonant energy transfer to FAD. The two main photoantennae found in CPF proteins are 5,10-methenyl-tetrahydrofolate (MTHF, Fig. 1, bottom right) and 8-hydroxy-7,8-didesmethyl-5-deazariboflavin (8-HDF, Fig. 1, top right, also known as F_0) [1,11]. MTHF was found in several CPD photolyases and cryptochromes-DASH, and 8-HDF in various CPD photolyases [12–15]. On the other hand (6-4) photolyases are consistently purified without photoantenna [16–20]. If a photoantenna is bound to (6-4) photolyases *in vivo* its nature is not yet known.

In this paper we report on the presence, nature and ultrafast photoinduced dynamics of a photoantenna in two recently discovered CPF proteins (OtCPF1 and OtCPF2) coming from the green alga *Ostreococcus tauri* [21]. OtCPF1 groups with the (6-4) photolyase and animal cryptochrome sub-family, and OtCPF2 is a cryptochrome-DASH. OtCPF1 is purified (after heterologous expression in *Escherichia coli*) without any photoantenna [19,22], while OtCPF2 is found to bind the photoantenna MTHF [22].

By using femtosecond broadband transient absorption spectroscopy, we studied the photoinduced resonance energy transfer between MTHF and FAD, within OtCPF2. Energy transfer from MTHF to FAD has already been reported for several CPF proteins [23–25]. We focus on comparing the energy transfer rates from MTHF to two different redox states of FAD: FAD_{ox}, the neutral oxidized form, and $FADH^-$, the anionic fully reduced form. Such a comparison was previously made by Saxena et al. [25] in the case of

* Corresponding author. Tel.: +33 144322414.
E-mail addresses: johanna.brazard@cea.fr (J. Brazard), christian.ley@uha.fr (C. Ley), fabien.lacombat@ens.fr (F. Lacombat), pascal.plaza@ens.fr (P. Plaza), laetitia.mony@berkeley.edu (L. Mony), marc.heijde@unige.ch (M. Heijde), zabulon@biologie.ens.fr (G. Zabulon), cbowler@biologie.ens.fr (C. Bowler).

1010-6030/$ – see front matter © 2012 Elsevier B.V. All rights reserved.
doi:10.1016/j.jphotochem.2012.01.012

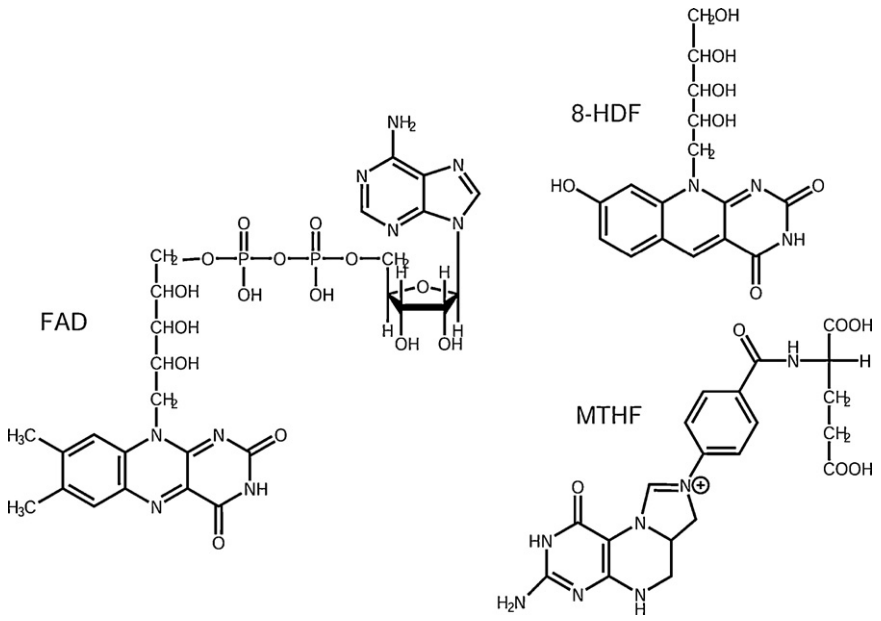

Fig. 1. Chemical structures of FAD (left), 8-HDF (top right) and MTHF (bottom right).

the cryptochrome-DASH of *Vibrio cholerae*, and lead the authors to propose a local change of the protein structure when the flavin is reduced from FAD_{ox} to $FADH^-$. We here reexamine this issue for OtCPF2 and confront it to structural information obtained by homology modeling.

For comparison we also studied the intrinsic photophysics of MTHF in aqueous solution, by femtosecond broadband transient absorption spectroscopy. Only one time-resolved fluorescence study on MTHF in water was previously reported [24]. The authors concluded to a fluorescence lifetime shorter than 30 ps, limited by the temporal resolution of their apparatus. They also showed that the excited-state lifetime of MTHF increases with the viscosity of the solvent.

Regarding the fact that OtCPF1 is purified without photoantenna, we used sequence alignment with other CPF proteins, as well as homology modeling, in order to propose a candidate photoantenna and give reasons for which the protein is purified without it.

2. Materials and methods

2.1. Sample preparation

OtCPF2 was overexpressed in *E. coli* as a GST (glutathione S-transferase) fusion protein. The expression and purification protocols have already been described elsewhere [22]. Briefly, purification was made on a Glutathione Sepharose 4B resin (Amersham Biosciences) which binds the GST tag. The protein was released by adding a GSH (reduced L-glutathione) rich elution buffer (Tris–HCl at pH 8.0 100 mmol L^{-1}, NaCl 100 mmol L^{-1}, GSH 20 mmol L^{-1}). The purified proteins were concentrated by means of Microcon centrifugable membrane filters (10 kDa cutoff) in order to obtain a final volume of 50 μL and a maximal absorbance (over 1 mm optical path) of 0.42 at 386 nm. After addition of glycerol (10%, v/v), they were stored at −80 °C.

MTHF (Schircks Laboratories) solution was dissolved in acidic (HCl) aqueous solution at pH 2.0, in order to prevent the hydrolysis of MTHF into 10-formyl-tetrahydrofolate (10-FTHF) [26]. The concentration of MTHF for transient absorption experiments was 170 μmol L^{-1}, corresponding to an absorbance over 1 mm optical path of 0.75 at the absorption maximum (352 nm).

2.2. Steady-state spectroscopy

UV–vis absorption spectra were recorded with double-beam UV spectrophotometers: UV-mc^2 (Safas). Fluorescence spectra were measured with a fully corrected Fluoromax-3 (Horiba Jobin-Yvon) spectrofluorimeter. The cell was thermostated at 5 °C by a temperature-controlled bath (Minichiller Inox, Huber).

2.3. Time-resolved absorption spectroscopy

Broadband (340–750 nm) femtosecond transient absorption spectra were recorded by the pump-probe with white-light continuum technique, as described elsewhere [27]. The laser source is a commercial amplified Ti:Sapphire laser system (Tsunami and Spitfire, Spectra Physics) delivering 50-fs pulses at 775 nm, at 1 kHz repetition rate. The 388-nm pump beam (55 fs, 0.13 μJ per pulse) was generated by focusing the 775 nm beam on a BBO crystal. The continuum probe beam was generated by focusing a few μJ per pulse of the 775-nm beam on a moving CaF_2 plate. The probe beam was then split into a sample beam and a reference beam. The pump and probe beams were focused on a diameter of about 80 μm onto the sample cell and crossed at an angle of *ca.* 5°. The probe beam was delayed with respect to the pump beam by a motorized optical delay line. The cuvettes were thermostated at 5 °C to prevent protein degradation, and continuously moved up and down in order to avoid photolysis. The probe beams (reference and sample) were dispersed in a spectrograph (Acton SP306i) and the spectra were recorded at 333 Hz on a CCD camera (Roper Scientific, Spec-10 100B, 100 × 1340 pixels). The linear polarizations of the pump and probe beams were set at the magic angle (54.7°).

The data were globally fitted to a sum of exponential functions and/or step function, after dimensional reduction and noise filtering by singular value decomposition (see technical details in Ref. [27]). Briefly, the fit functions were convoluted by a Gaussian function (100–130 fs FWHM) representing the instrument response function. In the first stage of analysis, the presence of a cross-phase modulation artifact during pump-probe overlap was empirically taken into account by adding the sum of the same Gaussian

function and its first and second time derivatives. In the final stage of analysis, times below ~200 fs were removed in order to minimize the interfering effects of the cross-phase modulation artifact. Such truncation reduced the effective time resolution of our setup and limited the analysis we could do of events occurring within the first couple hundred fs. The decay-associated difference spectrum (DADS, *i.e.* spectrum of pre-exponential factors) of each time component was calculated over the entire experimental spectral range.

We note that such global analysis is not well adapted to describe processes like solvation dynamics, characterized by a continuous time-dependent shift of the bands. Global analysis indeed tends to reduce the data to a collection of time-independent spectra, to each of which is attached a given kinetics. When the procedure is nevertheless applied to cases where time-dependent shift occur, some time constants must therefore be interpreted in terms of the underlying shift phenomenon.

2.4. Sequence alignment and homology modeling

Sequence alignments were generated with the online software ClustalW2 (EBI, http://www.ebi.ac.uk/Tools/clustalw2/index.html). These alignments were further manually refined according to secondary structures predicted using PROF predictions (http://www.predictprotein.org/) [28].

Reference CPF proteins for the alignments were: *E. coli* CPD photolyase (PDB code: 1DNP, noted EcCPD) [14], *Arabidopsis thaliana* cryptochrome 3 (PDB code: 2IJG, noted AtCry3) [13] and *Anacystis nidulans* CPD photolyase (PDB code: 1QNF, noted AnCPD) [15]. Complementary (6-4) photolyases used for the alignments were: *Drosophila melanogaster* (6-4) photolyase (noted Dm64), *Danio rerio* (6-4) photolyase (noted Dr64), *Xenopus laevis* (6-4) photolyase (noted Xl64), *Dunaliella salina* (6-4) photolyase (noted Ds64), and *A. thaliana* (6-4) photolyase (noted At64).

Homology models were subsequently generated by the automated comparative modeling tool MODELER 9.0 [29], in the DS Modeling 1.7 framework (Accelrys, San Diego, CA). Models were generated according to the previously generated alignment, and by using the coordinates of proper template structures (Dm64 [PDB code: 3CVU] [17] for OtCPF1 and AtCry3 [PDB code: 2IJG] for OtCPF2, as previously described in Ref. [22]). The structural quality of the models was assessed with MODELER 9.0 probability density functions and with Profiles-3D analysis (in DS Modeling 1.7).

Insertion of the 8-HDF photoantenna into OtCPF1 was performed using the following protocol: first, identification of the putative binding site of 8-HDF and initial positioning of the photoantenna in OtCPF1 was done by structural alignment of OtCPF1 homology model with the crystal structure of AnCPD (PDB code: 1QNF), which contains 8-HDF. The 8-HDF molecule was then docked in its putative binding-site using C-DOCKER (in DS modeling 1.7) [30].

3. Results

In the following subsections, we first report the intrinsic photophysical properties of MTHF in acidic aqueous solution, by femtosecond broadband transient absorption spectroscopy, in order to provide a useful reference on this molecule and compare with the primary events following excitation of MTHF in OtCPF2. We then present a study of the resonance energy transfer from MTHF to FAD in different redox states (FAD_{ox} and $FADH^-$), in OtCPF2. We finally report a theoretical study, by sequence alignment and homology modeling, of the possible nature of the photoantenna that OtCPF1 could hypothetically bind *in vivo*.

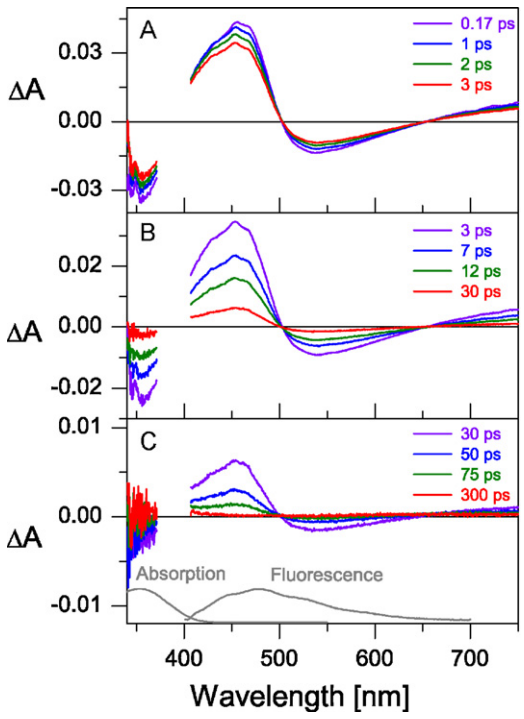

Fig. 2. Transient absorption spectra of MTHF in a buffer at pH 2.0 after excitation at 388 nm. The time evolution of the spectra between 0.17 and 3 ps is displayed in (A), between 3 and 30 ps in (B), and between 30 and 300 ps in (C). The steady-state absorption and fluorescence spectra of MTHF are recalled in gray lines in (C).

3.1. Transient absorption spectroscopy of MTHF in acidic aqueous solution

The concentration of MTHF (170 μmol L^{-1}) was chosen so as to achieve an absorbance over 1 mm optical path of 0.75 at the absorption maximum (352 nm) and 0.43 at the excitation wavelength (388 nm). Fig. 2 presents an overview of transient absorption spectra of MTHF, for pump-probe delays ranging from 0.17 to 300 ps. The steady-state absorption and fluorescence spectra of MTHF are recalled in gray lines in frame C.

At 0.17 ps delay (Fig. 2A) one observes two positive ΔA bands, dominated by transient absorption contributions: a large one from ~400 nm to 502 nm and a smaller one extending beyond 655 nm. Ground-state bleaching is seen around 350 nm and gives rise to a net negative band between 340 nm and about 370 nm, where it is dominant. Stimulated emission is apparent around 535 nm although superimposed to a transient absorption background. Stimulated emission is dominant, and produces a net negative signal, between 502 and 655 nm only.

The temporal evolution of the spectra shows three phases:

- Phase 1 (Fig. 2A): Between 170 fs and 3 ps, all bands are seen to start decaying. Meanwhile the transient absorption band around 450 nm undergoes a blue shift, of about 3 nm. During the same phase, no significant red shift of the stimulated band is observed.
- Phase 2 (Fig. 2B): Between 3 and 30 ps, one notes a large and fast decay of all the bands, which appears to be quasi-proportional (*i.e.* quasi-homothetic) at all wavelengths.
- Phase 3 (Fig. 2C): Between 30 and 300 ps, all bands decay toward zero, more slowly than in Phase 2, also in a quasi-proportional manner.

Global multiexponential analysis of the data was performed with best results by using three exponential components. The corresponding lifetimes were found to be: 0.70 ± 0.06 ps, 6.6 ± 0.2 ps

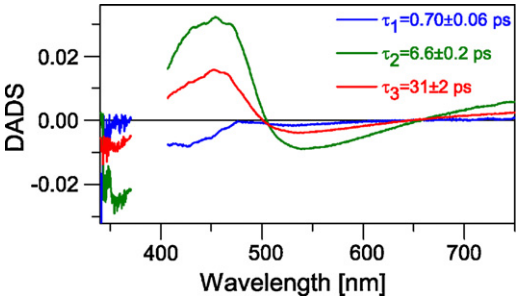

Fig. 3. DADS attached to each of the three time components found in the global analysis of the transient absorption spectra of MTHF, recorded after excitation at 388 nm.

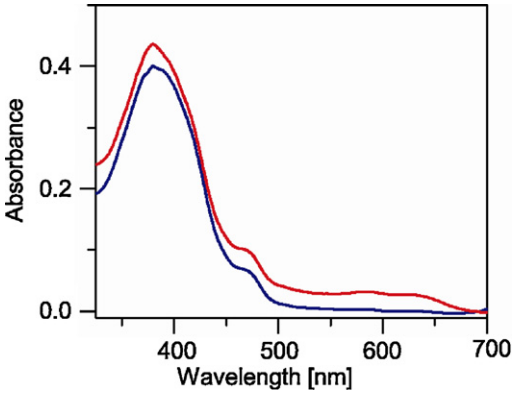

Fig. 4. Steady-state absorption spectra of samples OtCPF2-p (after purification; blue) and OtCPF2-o (after O_2 bubbling; red). (For interpretation of the references to color in this figure legend, the reader is referred to the web version of the article.)

and 31 ± 2 ps. The corresponding DADS (spectra of pre-exponential factors) are given in Fig. 3.

DADS1, attached with the lifetime of 0.70 ps, is closely related to the blue shift of the transient absorption band observed during Phase 1 (see above). As noted in Section 2.3, continuous band shifts are only crudely described by global analysis. However, it can be said that the 0.70 ps component essentially captures the existence of a phase characterized by a shift. Although no red shift of the stimulated-emission band was detected (possibly due to the overlap of the stimulated emission band by a transient absorption contribution) one may propose that solvation dynamics (relaxation of solvent molecules around MTHF in the excited state, triggered by some charge redistribution within the molecule) contributes to this ultrafast kinetic step. The lifetime of 0.70 ps is indeed rather close to the longest component of solvation dynamics of water (880 fs) [31]. We plotted the maximum of the 450-nm band (in wavenumber units) as a function of time in order to obtain a more detailed description of its blue shift. The result (see Supporting Information, Fig. S1) suggests a bi-exponential shift dynamics. The shortest component (*ca.* 70 fs) might be related to the fast solvation dynamics components of water (Gaussian component of frequency 38.5 ps^{-1} plus exponential component of 126 fs [31]). Alternatively or in addition, one may hypothesize that structural relaxation along low-frequency modes of the 1,2,3,4-tetrahydropyrazine ring could also contribute to the ultrafast excited-state behavior of MTHF in water solution.

The other two DADS are positive in the transient absorption domains and negative in the bleaching and stimulated emission domains. These spectral features sign the decay of excited-state species with concomitant ground-state recovery. DADS2 (attached to the lifetime of 6.6 ps) and DADS3 (31 ps) have similar shapes but DADS2 is roughly twice as large as DADS3. Moreover DADS3 is less broad than DADS2 in the transient absorption band around 450 nm and in the stimulated-emission band after normalization at the maximum of the transient absorption band (see Supporting Information, Fig. S2).

3.2. Steady-state spectroscopy of OtCPF2. Effect of dioxygen bubbling

As previously reported, OtCPF2 non-covalently binds two chromophores: the photoantenna MTHF and the cofactor FAD [22]. OtCPF2 is purified in a mixture of identical proteins bearing FAD in different redox states (neutral oxidized FAD_{ox}, neutral semi-reduced $FADH^{\bullet}$, and anionic fully reduced $FADH^{-}$). In order to help differentiating energy transfer from MTHF to the redox states of FAD, transient absorption experiments were carried out on two different OtCPF2 samples. The first one was obtained after purification and concentration, without any further treatment; it is here called OtCPF2-p. The second sample was obtained after bubbling dioxygen in OtCPF2-p; it is called OtCPF2-o. The steady-state absorption spectra of both samples are shown in Fig. 4. The MTHF concentration in both OtCPF2 samples was similar ~110 $\mu mol\ L^{-1}$.

The effect of dioxygen bubbling is to decrease the ratio of reduced to oxidized forms of FAD. This was quantified by fitting the absorption spectra of the OtCPF2-p and OtCPF2-o samples by a sum of reference spectra of FAD_{ox}, $FADH^{\bullet}$, $FADH^{-}$ and MTHF, as previously described in Ref. [22].

The distribution of FAD redox states within OtCPF2-p was found to be: $21.0 \pm 0.5\%$ FAD_{ox}, $4.6 \pm 0.8\%$ $FADH^{\bullet}$ and $74.4 \pm 1.0\%$ $FADH^{-}$. This corresponds to the following concentrations: $[FAD_{ox}] = 54.4 \pm 0.7\ \mu mol\ L^{-1}$, $[FADH^{\bullet}] = 12 \pm 2\ \mu mol\ L^{-1}$ and $[FADH^{-}] = 193 \pm 2\ \mu mol\ L^{-1}$. The coefficient of determination R^2 of the fit (fitting goodness) was 0.9996. The ratio of MTHF concentration ($109.0 \pm 0.4\ \mu mol\ L^{-1}$) to the total concentration of the FAD ($260 \pm 5\ \mu mol\ L^{-1}$) was $42 \pm 1\%$.

After O_2 bubbling, the composition of sample OtCPF2-o was: $22.6 \pm 0.5\%$ FAD_{ox}, $8.7 \pm 0.5\%$ $FADH^{\bullet}$ and $68.7 \pm 0.7\%$ $FADH^{-}$. The corresponding concentrations were: $[FAD_{ox}] = 57.1 \pm 0.6\ \mu mol\ L^{-1}$, $[FADH^{\bullet}] = 22 \pm 1\ \mu mol\ L^{-1}$ and $[FADH^{-}] = 173 \pm 2\ \mu mol\ L^{-1}$. R^2 of this fit was 0.9998. The ratio of MTHF concentration $111.0 \pm 0.3\ \mu mol\ L^{-1}$ to the total concentration of FAD $252 \pm 4\ \mu mol\ L^{-1}$ was $44 \pm 1\%$.

It appears that O_2 bubbling induces the following changes of molar ratios: slight increase of FAD_{ox}, increase of $FADH^{\bullet}$ and, mostly, decrease of $FADH^{-}$. These changes are small but however larger than twice the corresponding errors. They should therefore be considered significant.

3.3. Transient absorption spectroscopy of OtCPF2 upon excitation of MTHF

The transient absorption spectroscopy of OtCPF2-p after excitation at 388 nm excitation is reported first. Given its ground-state composition, the primary excited-state composition (*i.e.* before any spontaneous evolution) of this sample is the following: 70% MTHF*, 17% $FADH^{-}$*, 11% FAD_{ox}* and 2% $FADH^{\bullet}$* (star labeling indicates the excited state). Percentages are given relative to the total concentration of excited species (FAD and MTHF). They show that irradiation at 388 nm essentially excites MTHF.

Fig. 5 displays the transient absorption spectra of OtCPF2-p for pump-probe delay ranging from 130 fs to 1.4 ns. At 130 fs two net negative bands are observed: one extends between 340 and 418 nm and is dominated by the bleaching of MTHF, while the second one, lying between 510 and 638 nm, arises from stimulated emission of MTHF. Two positive bands dominated by transient absorption are observed between 418–510 nm and 638–750 nm.

The temporal evolution of the spectra shows three phases:

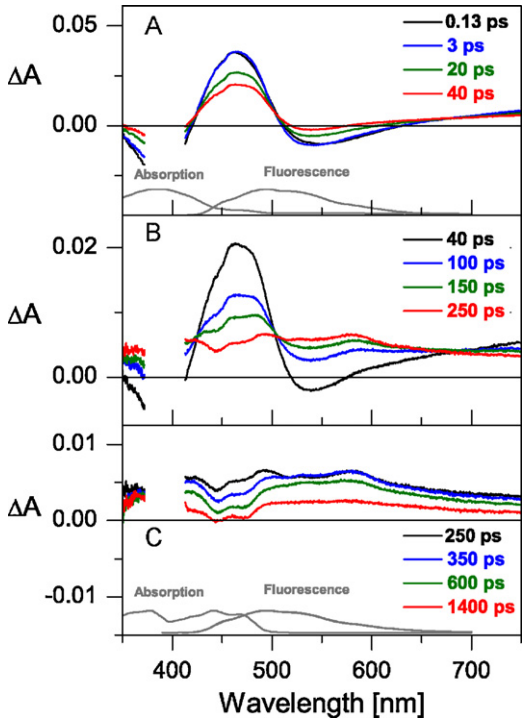

Fig. 5. Transient absorption spectra of OtCPF2-p in Tris buffer after excitation at 388 nm. The time evolution of the spectra between 0.13 and 40 ps is displayed in frame (A), between 40 and 250 ps in (B), and between 250 and 1400 ps in (C). The steady-state absorption and fluorescence spectra of OtCPF2-p are recalled in gray lines in (A). The steady-state absorption spectrum of FAD_{ox} in *Escherichia coli* CPD photolyase [32] and emission spectrum of OtCPF2 are displayed in gray lines in (C).

- Phase 1 (Fig. 5A): Between 130 fs and 40 ps, all bands substantially decay. This decay is however non-proportional (non homothetical) at all wavelengths as shows the presence of three non trivial (*i.e.* $\Delta A \neq 0$) temporary isosbestic points at 423 nm, 504 nm and 677 nm. A clear narrowing of the stimulated emission band is additionally visible on its red side.
- Phase 2 (Fig. 5B): Between 40 and 250 ps, one notes that the negative bands disappear, replaced by broad positive signals. A shallow maximum appears at 580 nm. A dip is clearly seen to grow within the main blue transient absorption band, at 445 nm. A second dip becomes visible around 475 nm. The negative bleaching band of MTHF is concomitantly replaced by a featureless positive background.
- Phase 3 (Fig. 5C): Between 250 ps and 1.4 ns, the bands observed at the end of phase 2 decay while the dip at 475 nm becomes clearer. Some residual signal is still seen at 1.4 ns, showing a very broad, positive transient absorption background with local minima at 445 nm and 475 nm. It should be noted that those minima correspond to absorption maxima of FAD_{ox} in the enzyme (see steady-state absorption spectrum of FAD_{ox} in *E. coli* CPD photolyase [32] in Fig. 5C, gray line). They should therefore be considered as a bleaching band resulting from the excitation of FAD_{ox}.

Global analysis performed of the transient absorption spectra of OtCPF2-p yielded the following time constants: $\tau_1 = 17.3 \pm 0.7$ ps, $\tau_2 = 108 \pm 4$ ps, $\tau_3 = 548 \pm 39$ ps and $\tau_4 = \infty$ (*i.e.* step function). Fig. 6A shows the corresponding DADS.

DADS1 (attached to the lifetime of 17.3 ps) shows negative signal in the areas of bleaching and stimulated emission of MTHF and a positive signal in the transient absorption band between them. One notes a positive bump around 447 nm. The shapes of DADS2 (attached to the lifetime of 108 ps) and of DADS1 are similar, but not identical as seen after normalization (data not shown), especially beyond 500 nm. DADS2 is globally larger than DADS1, in particular at 465 nm. Moreover DADS2 does not show any specific feature at 447 nm. DADS3 (548 ps) is positive at all wavelengths. Dips (valleys) may be seen below 425 nm, around 450 nm and above 590 nm. Correspondingly shallow local maxima are observed around 450 nm, and between 515 and 550 nm. DADS4 shows a broad positive background almost everywhere on which two dips at 445 nm and 475 nm superimpose, reaching negative values.

3.4. Transient absorption spectroscopy of OtCPF2 after O_2 bubbling

Upon 388 nm excitation, the initial excited-state composition (before any spontaneous evolution) of each sample OtCPF2-o (obtained after O_2 bubbling; see Section 3.2) is the following: 71% MTHF*, 15% $FADH^{-}$*, 11% FAD_{ox}* and 3% $FADH^{\bullet}$*. The excited-state distribution of OtCPF2-o is similar to that of OtCPF2-p and is still dominated by MTHF*. The main difference between the two samples is the decrease of the $FADH^{-}$ fraction in OtCPF2-o. The excitation conditions (wavelength, energy, area) were identical in both cases.

The transient absorption spectra of OtCPF2-o (given as Supporting Information, see Fig. S3) are similar to those of OtCPF2-p (Fig. 5) and show similar evolution. One in particular still observes three temporary isosbestic points, at 423 and 504 and 677 nm, for pump-probe delays between 0.38 and 40 ps. The bleaching and stimulated emission bands of MTHF still disappear between 40 and 250 ps, replaced by broad positive signals, while dips at 445 and 475 nm are seen to grow and remain visible at 1400 ps. The main difference observed is the largest amplitude of the two minima for OtCPF2-o. At 1400 ps, one can in particular observe that they reach net negative values (Fig. S3), which was barely the case for OtCPF2-p (Fig. 5).

Global analysis performed of the transient absorption spectra of OtCPF2-o yielded the following time constants: $\tau_1 = 13 \pm 1$ ps, $\tau_2 = 91 \pm 9$ ps, $\tau_3 = 538 \pm 161$ ps and $\tau_4 = \infty$ (step function). These lifetimes are almost identical to those of OtCPF2-p. Fig. 6B shows the corresponding DADS. The shapes of those spectra are very similar to the corresponding ones of OtCPF2-p (Fig. 6A). One however notes some differences, induced by O_2 bubbling:

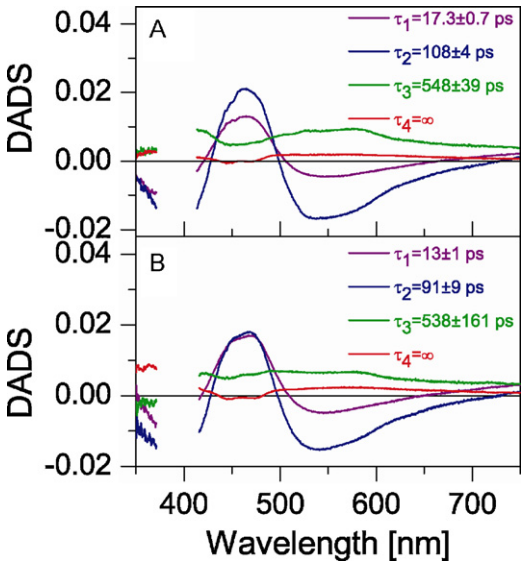

Fig. 6. DADS attached to each of the four time components found in the global analysis of the transient absorption spectra of OtCPF2-p (after purification; frame A) and OtCPF2-o (after O_2 bubbling; frame B), recorded under excitation at 388 nm.

- DADS1 and DADS2 (associated to the lifetimes of 13 and 91 ps, respectively) have comparable amplitude at 465 nm for OtCPF2-o, while the amplitude of DADS2 was larger than that of DADS1 at this wavelength for OtCPF2-p.
- DADS3 (538 ps) presents a smaller amplitude for OtCPF2-o than for OtCPF2-p.
- DADS4 (step function) is conversely larger and the two minima at 445 and 475 nm are more pronounced.

3.5. Sequence alignment and homology modeling of OtCPF1

We report in this section sequence alignment and homology modeling studies on OtCPF1, aimed at shedding light on the chemical nature of the photoantenna that this protein might bind *in vivo*. Let us indeed recall that OtCPF1, a (6-4) photolyase, is purified without any secondary chromophore [19,22].

Whereas the FAD cavity is well conserved in CPF proteins [1], the binding site for the photoantenna significantly changes according to the type of protein. At least three different patterns are known [1]. The main differences are seen between CPF proteins that bind MTHF (*e.g. E. coli* CPD photolyase [14], noted EcCPD, or *A. thaliana* cryptochrome 3 [12], noted AtCry3) and those that bind 8-HDF (*e.g. A. nidulans* CPD photolyase [15], noted AnCPD). In addition, the binding site for MTHF further changes between CPD photolyases (*e.g.* EcCPD) and cryptochromes-DASH (*e.g.* AtCry3) [13].

We carried out a search of conserved amino acids in the region of photoantenna binding between OtCPF1 and representatives of the three types of binding patterns. Our base of comparison was EcCPD for MTHF binding of the first type, AtCry3 for MTHF binding of the second type, and AnCPD for 8-HDF binding. This choice is justified by the fact that the photoantenna sites are fully characterized by crystallography in these three cases, which allows precise identification of the amino acids involved in binding. The alignment of the full amino acids sequence of OtCPF1 to those of the three reference proteins was done separately. For each alignment other (6-4) photolyases (Dm64, Dr64, Xl64, Ds64, At64) were added to OtCPF1 in order to evaluate if common binding features could be found across this particular CPF sub-family. The full names of those complementary (6-4) photolyases are listed in Section 2.4.

Only one conserved amino acid (in the region of photoantenna binding) was found between OtCPF1 and EcCPD alone (see Supporting Information, Fig. S4), and none between OtCPF1 and AtCry3 alone (Supporting Information, Fig. S5). It thus appears unlikely that OtCPF1 could bind MTHF *in vivo*.

Much more conserved amino acids (in the region of photoantenna binding) are found upon comparison to AnCPD. Fig. 7 shows the alignment of OtCPF1, and of five other (6-4) photolyases, to AnCPD. Nine common amino acids can be counted between OtCPF1 and AnCPD alone, and six common amino acids (highlighted by red triangles in Fig. 7) in the full group of seven proteins.

Given the fact that a relatively large number of conserved amino acids were found between OtCPF1 and AnCPD in the region of photoantenna binding, we examined by homology modeling if a satisfactory 3D model of 8-HDF binding to OtCPF1 could be found. First a homology model of OtCPF1 was generated, using Dm64 (*D. melanogaster* (6-4) photolyase, PDB code: 3CVU) as a template. Since the crystallographic structure of Dm64 does not include 8-HDF, this photoantenna was inserted in a second time into the OtCPF1 model by docking, using the crystallographic structure of AnCPD as a guide (see Section 2.4). The main amino acids in interaction with 8-HDF in AnCPD are displayed in Fig. 8, left. Fig. 8, right, shows the corresponding case of OtCPF1, according to our homology modeling. It appears that both cases are very similar. As will be further discussed in Section 4.4, this similitude confirms the above-mentioned strong conservation of amino acids between AnCPD and OtCPF1 in the region of photoantenna binding, and supports the hypothesis that the natural photoantenna of OtCPF1 *in vivo* could be 8-HDF.

4. Discussion

4.1. Photodynamics of free MTHF in aqueous solution

Global multiexponential analysis of the transient absorption data of free MTHF in aqueous solution yielded three exponential decays of 0.70 ps, 6.6 ps and 31 ps (see Section 3.1). The sub-picosecond component was already assigned to either solvation dynamics or structural relaxation, or any combination of those phenomena. As far as the 2 ps decays are concerned, let us recall that the corresponding spectra of pre-exponential factors (DADS2 and DADS3) have similar shapes, DADS3 displaying slightly narrower transient absorption (around 450 nm) and stimulated-emission bands. The relative weights of the 6.6 ps and 31 ps components (*i.e.* DADS2/(DADS2 + DADS3) and DADS3/(DADS2 + DADS3)) are somewhat dependent on wavelength but average values can be estimated: about 30% for the 6.6 ps component and about 70% for the 31 ps component. Whatever the exact nature of these two decays it must be underlined that the excited-state decay of MTHF is globally very fast and thus corresponds to some efficient quenching pathway. No trace of concomitant formation, with substantial yield, of any photoproduct (*e.g.* triplet state) is apparent in our measurement.

The photodynamic behavior of free MTHF bears some resemblance with that of $FADH^-$, the anionic fully reduced form of FAD, in aqueous solution. Several time-resolved studies [33–37] report a multiexponential decay of the excited state of $FADH^-$. Brazard et al. in particular showed that upon one-photon excitation $FADH^-$ undergoes a biexponential decay of about 5 and 30 ps, the DADS of which having comparable shapes but the second one exhibiting narrower and blue-shifted bands [36]. One may note that the weights of the two decay constants for MTHF are similar to those reported by Zhao et al. [37] in the case of $FADH^-$, but different from those of $FADH_2$. Several authors invoked the role of the flexibility of the molecule, especially the "butterfly" motion (bending about the N5–N10 axis) which interconverts two boat conformers. Li et al. [35] attributed two fast decays of $FADH^-$ to the presence of two butterfly conformers of the isoalloxazine ring, and Kao et al. [34] attributed the multiexponential decay to a deactivation mechanism occurring by butterfly bending motion across conical intersections.

One first hypothesis is that the bimodal decay of MTHF could arise from two different MTHF conformers. One could speculate that the difference between the two conformers could be due to the structure of the 1,2,3,4-tetrahydropyrazine ring. This line of interpretation would be similar to the one of Li et al. in the case of $FADH^-$ [35]. It should at this point be mentioned that Kim et al. [24] previously reported that the excited-state lifetime of MTHF increases in more viscous solvents. This observation evokes the possibility that some large amplitude molecular motion is involved in the quenching mechanism, like for molecular rotors for instance [38,39]. Within the two-conformer hypothesis, the internal coordinate that allows switching between the two conformers could be thought to play the role of quenching pathway.

In a related but different point of view one could follow the line proposed by Kao et al. for $FADH^-$ [40], that is, to invoke the crossing of a conical intersection found along an excited-state pathway involving some large amplitude molecular motion. In the case of MTHF this motion could be related to the flexibility of the 1,2,3,4-tetrahydropyrazine ring. It is in this respect most interesting to recall that Kim et al. [24] observed the excited-state lifetime of MTHF increases with the viscosity of the solvent and that it becomes rather large (354 ps) upon binding to a CPD photolyase. Saxena

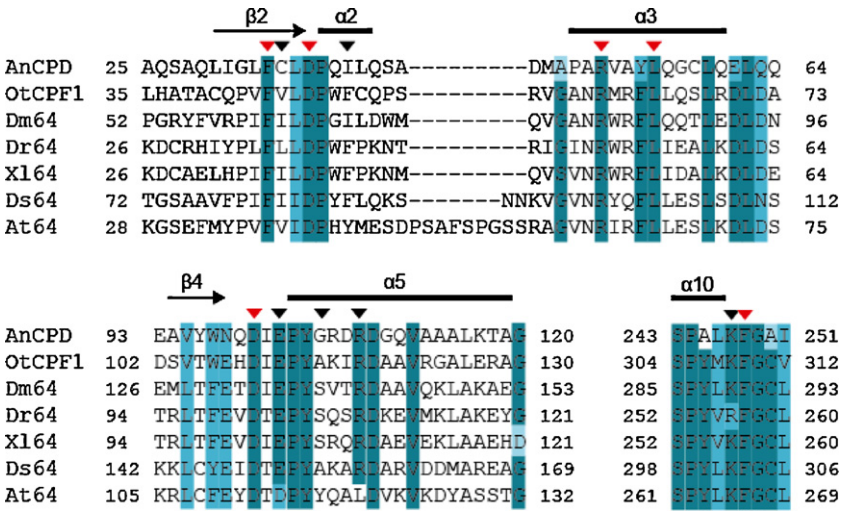

Fig. 7. OtCPF1 and the (6-4) photolyases share high sequence homology with AnCPD in the regions lining 8-HDF binding-site. The secondary structure elements are derived from the crystal structure of AnCPD (PDB code: 1QNF). Identical and similar residues are shaded in blue: dark blue, identity; medium blue, strong homology; light blue, weak homology. The triangles represent the positions of the residues contacting 8-HDF in the crystal structure of AnCPD: red triangles, positions at which the residues are identical between AnCPD and all the photolyases; black triangles, other positions. (For interpretation of the references to color in this figure legend, the reader is referred to the web version of the article.)

et al. demonstrated an even longer excited-state lifetime of MTHF (845 ps) when it is bound to a cryptochrome-DASH [25]. These elements support the hypothesis that the environment constraints control excited-state deactivation of MTHF, possibly through its internal flexibility.

4.2. Förster resonant energy transfer within OtCPF2

In Sections 3.3 and 3.4 we have shown that, upon dominant excitation of MTHF at 388 nm, the transition absorption behavior of OtCPF2 exhibits three exponential components followed by a plateau. The time constants found for the OtCPF2-p and OtCPF2-o samples are essentially identical, with values of about 15 ps, 100 ps and 550 ps. The corresponding DADS also have nearly identical shapes. The main difference is that upon O_2 bubbling, which reduces the amount of $FADH^-$ in the sample, the relative amplitude of DADS2 (100 ps) decreases relatively to the one of DADS1 (15 ps).

Similar time constants were reported by Saxena et al. [25] in the case of *V. cholerae* cryptochrome 1 (VcCry1), a cryptochrome-DASH containing MTHF like OtCPF2, upon excitation at 400 nm. These authors found two components of 10 ps and 60 ps, which they assigned to energy transfer from excited MTHF to FAD_{ox} and $FADH^-$, respectively.

If the same interpretation should be applied to the 15 ps and 100 ps components of this work, the spectral signature of the new species produced by energy transfer should appear in the DADS attached to these time constants. Indeed, in the simple case where the energy acceptor does not evolve after energy transfer, the DADS attached to the energy transfer time is expected to be the difference of two terms. The first term is the transient absorption spectrum of the energy donor (decaying) and the second one is the transient absorption spectrum of the acceptor (rising), multiplied by the reaction yield.

Both DADS1 and DADS2 clearly contain the spectral signature of excited MTHF, as one can see by referring to Fig. 2 of Section 3.1, but they are however not identical. DADS1 (15 ps) shows a specific positive bump centered around 447 nm which corresponds to a local maximum of the steady-state absorption spectrum of FAD_{ox} bound to the protein. This feature is interpreted as signing the rise of the bleaching of FAD_{ox}, which in turn allows assigning the 15-ps component to energy transfer from excited MTHF to FAD_{ox}. In DADS2 the main difference with the signature of excited MTHF is an additional negative broad band between 500 and 600 nm. This

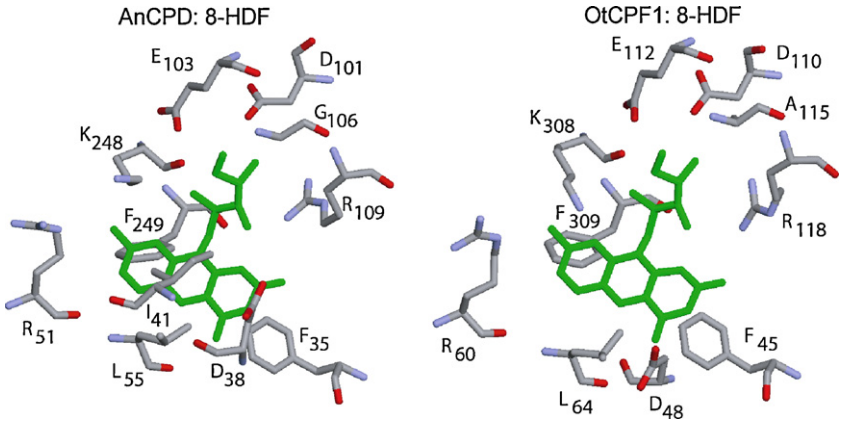

Fig. 8. Photoantenna binding-sites of AnCPD [15] (left) and OtCPF1 (right) as calculated by molecular modeling. 8-HDF is represented in green. (For interpretation of the references to color in this figure legend, the reader is referred to the web version of the article.)

superposition is in particular responsible for the shoulder observed around 600 nm. It is attributed to the rise of transient absorption spectrum of excited $FADH^-$, which indeed exhibits a positive band in the 500–600 nm region [24,36]. This feature allows assigning the 100-ps component to energy transfer from excited MTHF to $FADH^-$. After O_2 bubbling, which decreases the fraction of $FADH^-$ in the sample, the relative amplitude of DADS2 decreases with respect to that of DADS1. This effect confirms our assignment of the 15 ps and 100 ps lifetimes to the energy transfer from excited MTHF to FAD_{ox} and $FADH^-$, respectively.

One notes that energy transfer from MTHF is slower to $FADH^-$ than to FAD_{ox}, as already observed for VcCry1 [25]. We will see below that this observation is mainly understood in terms of the spectral overlap between the emission spectrum of the energy donor and the absorption spectrum of the energy acceptor. The corresponding overlap integral is larger in the case of MTHF–FAD_{ox} than for MTHF–$FADH^-$. A more subtle effect can be found in a variation of the orientation factor upon changing the redox state of FAD. A similar difference, between energy transfer from MTHF to $FADH^-$ (292 ps) and to $FADH^\bullet$ (19 ps), has been reported for *E. coli* photolyase [41].

According to Förster's theory of resonant energy transfer [42,43], the rate of energy transfer (k_{ET}) is proportional to the product of an overlap integral (J) between the emission spectrum of the donor and the absorption spectrum of the acceptor and an orientation factor (κ^2) quantifying the relative orientation of the donor and acceptor molecules. This rate is also inversely proportional to the sixth power of the distance (r) between donor and acceptor. Förster's theory is applicable provided that r is larger than 1 nm [42]. This condition is fulfilled in our case because the distance between MTHF and FAD, as calculated by homology modeling [22], is of the order of 1.55 nm.

By using Förster's theory, it is possible to give a theoretical expression of the ratio of the rates corresponding to energy transfer from excited MTHF to FAD_{ox} and to $FADH^-$. Since the energy donor is the same in both cases this ratio reduces to the following simple expression, where the "ox" attribute refers to energy transfer to FAD_{ox} and the "red" attribute refers to energy transfer to $FADH^-$:

$$\frac{k_{ET}^{ox}}{k_{ET}^{red}} = \left[\frac{\kappa_{ox}^2 \times J^{ox}}{\kappa_{red}^2 \times J^{red}}\right] \times \left[\frac{r^{red}}{r^{ox}}\right]^6 \quad (1)$$

This relation allows us calculating the ratio of orientation factors corresponding to the two energy transfers, which is interesting to evaluate if any modification of the donor/acceptor relative orientation can be distinguished when FAD is reduced from FAD_{ox} to $FADH^-$. In order to obtain k_{ET} we used the corresponding time constant measured by transient absorption experiment (τ_{ET}), corrected from the intrinsic decay of MTHF within the protein if energy transfer did not take place (τ_{MTHF}) as follows:

$$k_{ET} = \frac{1}{\tau_{ET}} - \frac{1}{\tau_{MTHF}} \quad (2)$$

The intrinsic τ_{MTHF} decay has not been measured for OtCPF2 but two values have been reported in the literature, 354 ps for EcCPD [24] and 845 ps for VcCry1 [25]. As mentioned in Section 3.5, the binding site of MTHF changes according to the type of protein, in particular between CPD photolyases and cryptochromes DASH. Since VcCry1 is a cryptochrome-DASH as OtCPF2 and EcCPD is a CPD photolyase, we chose the decay reported for the protein bearing higher similarity with OtCPF2, *i.e.* VcCry1. It is incidentally interesting to observe that this lifetime is much longer that the excited-state lifetime of free MTHF in solution (see Section 3.1). This may be understood as the effect of the protein environment blocking the molecular motions responsible for the excited-state quenching of free MTHF in solution (see Section 4.1). By using τ_{MTHF} = 845 ps the energy transfer rates were calculated to be $6.55 \times 10^{10}\ s^{-1}$ for the FAD_{ox} case and $8.82 \times 10^{9}\ s^{-1}$ for the $FADH^-$ case, and the corresponding quantum yields of energy transfer ($1 - \tau_{ET}/\tau_{MTHF}$) to be 98% and 88%, respectively. The distances between MTHF and FAD_{ox} or $FADH^-$ were calculated from a homology model reported elsewhere [22] and the overlap integrals were calculated from reference spectra of MTHF, FAD_{ox} and $FADH^-$ bound to EcCPD [32].

The ratio $Q = \kappa_{red}^2/\kappa_{ox}^2$ of orientation factors is finally found to be 1.2.

This value is lower than the one (1.7) reported by Saxena et al. [25] but it should be mentioned that these authors did not take into account the intrinsic decay of MTHF in their calculations. If we follow their method, we obtain a ratio of 1.6, which is very close to their value. The fact that ratio Q is larger than one might be attributed to some protein reorganization. Since FAD_{ox} is a neutral chromophore and $FADH^-$ is a charged one, it may indeed be suspected that the surrounding amino acids reorganize upon changing the charge of the flavin. We checked this hypothesis by homology modeling, optimizing a model of OtCPF2 in two cases: OtCPF2 binding FAD_{ox} and OtCPF2 binding $FADH^-$ (data not shown). No major difference of the relative orientation of FAD and MTHF was however noticed in the two optimized models. Another factor affecting ratio Q is the fact that κ^2 actually measures the relative orientation of the emission transition dipole moment of the energy donor and the absorption transition dipole moment of the energy acceptor. Interestingly it has been shown that the transient absorption dipoles of FAD_{ox} [44] and $FADH^-$ [45] are not parallel; there in fact is an angle of about 50° between them. We tried to use the two above-mentioned optimized models and calculate Q by taking into account the angle between the transient absorption dipoles. We found a value of Q lower than one, which is inconsistent with the ratio obtained from the experimental data. We finally conclude that (i) the reorganization of the protein upon going from FAD_{ox} to $FADH^-$ must be the dominant effect explaining the experimental value of Q, (ii) and that our homology optimized models failed to reveal it.

From the above experimental results we finally extracted the critical distance of energy transfer R_0, or Förster radius, using the following classical relation:

$$R_0 = r(k_{ET}\tau_{MTHF})^{1/6} \quad (3)$$

We found R_0 = 3.03 nm for the MTHF–FAD_{ox} pair and R_0 = 2.17 nm for MTHF–$FADH^-$. This latter value is larger than the one reported by Saxena et al. [41] for MTHF–$FADH^-$ in *E. coli* CPD photolyase (1.735 nm). As understandable from (3), this difference is mostly due to the fact that τ_{MTHF} chosen in this work (845 ps) is much longer than the one measured by Saxena et al. (354 ps). Again, this choice comes from the fact that the binding site for MTHF in a cryptochrome-DASH like OtCPF2 is expected to be different from the one in a CPD photolyase.

4.3. Full kinetic model of the photodynamic behavior of OtCPF2

Going back to the photodynamic behavior of OtCPF2 it may be noted that DADS3, associated to the 550-ps time component, does not show any negative signal. It is a very broad positive continuum with local maxima around 450 nm, and between 515 and 550 nm. This spectrum strongly reminds the transient absorption spectrum of excited $FADH^-$ bound to EcCPD, reported by the group of Mataga [24,46] and also that of free excited $FADH^-$ in solution [36]. DADS3 is therefore attributed to the decay of $FADH^-$ excited by energy transfer from MTHF.

DADS4 shows two local minima at 447 and 475 nm which are attributed to FAD_{ox} bleaching, hence FAD_{ox} excitation, resulting

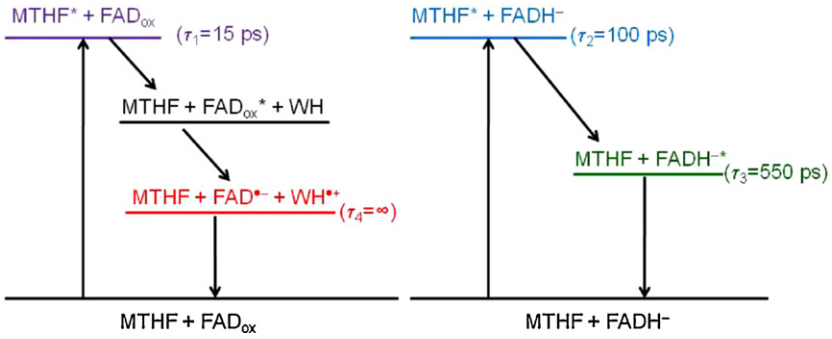

Fig. 9. Kinetic model proposed to describe the energy transfer from MTHF to FAD_{ox} and $FADH^-$ in OtCPF2.

from energy transfer from MTHF. It was previously shown that excited FAD_{ox} bound to OtCPF2 decays in 590 fs and gives rise to photoproducts of the reduction of FAD_{ox} ($FAD^{\bullet -}$ and tryptophanyl radicals) [22]. The rise of these photoproducts is not observed here because the energy transfer is much slower than this reaction. DADS4 is therefore the spectral signature of the photoproducts. One more proof is that, after O_2 bubbling, the two minima are more pronounced. This is due to a larger concentration of excited FAD_{ox} produced by energy transfer from MTHF and confirms that DADS4 is the spectral signature of the photoproducts of $FAD_{ox}{}^*$.

The above considerations added to the discussions of Section 4.2 allow us proposing a comprehensive kinetic model of the photodynamic behavior of OtCPF2 after preferential excitation of MTHF at 388 nm, depicted in Fig. 9.

4.4. Putative photoantenna of OtCPF1 in vivo

We have shown in Section 3.5 that only one conserved amino acid was found between OtCPF1 and EcCPD alone in the region of photoantenna binding, and none between OtCPF1 and AtCry3 alone. This poor homology between OtCPF1 and MTHF-binding CPF protein, in the region of MTHF binding, strongly suggests that OtCPF1 does not bind MTHF *in vivo*. Furthermore it has been shown in the case of AtCry3 that mutating glutamic acid 149 (E_{149}) to alanine induces the loss of MTHF [47]. In OtCPF1 this determinant amino acid is a tyrosine with a larger steric hindrance than the glutamic acid. This fact supports our conclusion that MTHF is probably not the natural photoantenna of OtCPF1.

On the contrary we have found nine conserved amino acids between OtCPF1 and AnCPD, in the region of 8-HDF binding, and six conserved amino acids in the group of six (6-4) photolyases including OtCPF1 and AnCPD (see Fig. 7). This strong homology suggests that the natural photoantenna of OtCPF1 *in vivo* could well be 8-HDF. One could even speculate that the other (6-4) photolyases, which have been purified without secondary cofactor, might also bind 8-HDF *in vivo*, as it has already been suggested [11,20]. By homology modeling with insertion of 8-HDF (Fig. 8), we have shown that the tertiary structure of OtCPF1 (as approximated by homology modeling) is compatible with 8-HDF binding and that the structure of the complex is very similar to the one of AnCPD (as revealed by X-ray diffraction [15]). It may additionally be noted that Lysine 308 (K_{308}), which is crucial to the stabilization of 8-HDF by hydrogen bonding [15], is conserved in OtCPF1 and putatively in a configuration that allows proper interaction with 8-HDF. The above elements concur in confirming the hypothesis that OtCPF1 could bind a photoantenna *in vivo* and that this molecule would be 8-HDF.

The question should then be asked as to why OtCPF1, as other (6-4) photolyases, was overexpressed and purified without secondary cofactor. One could evoke the possibility that the photoantenna is simply lost during the purification procedure, because the corresponding binding constant is not large enough. If 8-HDF was the natural photoantenna of OtCPF1, one would however expect the complex to be quite stable because the binding site of 8-HDF is known to be deeply buried inside the protein, even more so than the MTHF site of MTHF-binding CPF proteins [15]. Takao et al. interestingly noted that AnCPD bears the photoantenna 8-HDF *in vivo* but does not bear it anymore after overexpression in *E. coli* [48]. The authors concluded that 8-HDF is not available in *E. coli*, which thus does not allow the formation of the corresponding complex with AnCPD. The complex could however be successfully reconstituted after overexpression of AnCPD in *E. coli* when 8-HDF was added in a final step of purification [23]. Since OtCPF1 was overexpressed in *E. coli* in our study, without external addition of 8-HDF, the same argument could hold and explain why our OtCPF1 samples do not contain any photoantenna.

5. Conclusion

This study allowed us to spectrally fully characterize the energy transfer from MTHF to FAD_{ox} or $FADH^-$ in OtCPF2, a newly purified cryptochrome-DASH from *O. tauri*. Those two energy transfers occur in 15 ps and 100 ps, respectively. The analysis of the experimental data according to a FRET model revealed that some reorganization of the protein likely occurs when FAD is reduced from FAD_{ox} to $FADH^-$, inducing a change of the relative orientation of MTHF and FAD. Two additional time components were detected and attributed to the dynamics of excited $FADH^-$ and FAD_{ox}. Excited $FADH^-$ is seen to decay in 550 ps. As far as FAD_{ox} is concerned, it was previously showed that excited FAD_{ox} is very rapidly reduced by a nearby tryptophan residue in OtCPF2 and decays in 590 fs [22]. Since in the present study FAD_{ox} is excited by energy transfer in 15 ps, this ultrafast step could not be detected and only the resulting photoproducts ($FAD^{\bullet -}$ and tryptophanyl radicals) were observed as a long-lived component (plateau).

Our study of energy transfer in OtCPF2 in particular showed that the intrinsic lifetime of excited MTHF in OtCPF2 is at least longer than the slowest energy transfer time (to $FADH^-$), that is, 100 ps. The intrinsic lifetime of excited MTHF was in fact found to be 845 ps in VcCry1, as reported by Saxena et al. [25]. These values are in contrast with the much faster excited-state decay of free MTHF in acidic aqueous solution (6.6 and 31 ps). This difference supports our proposal that the excited-state decay of free MTHF in solution is due to the existence of some large-amplitude motions linked to the flexibility of the 1,2,3,4-tetrahydropyraxine ring. The bimodal decay of excited free MTHF might as well be interpreted as the photodynamics of two different conformers. In any case complexation of MTHF to the enzyme would hinder the aforementioned motions and increase the intrinsic lifetime of MTHF, in a similar way as previously proposed for $FADH^-$ bound to a photolyase or cryptochrome [33–36,40].

Finally, our study allowed us proposing a reason why OtCPF1, a (6-4) photolyases extracted from *O. tauri*, is purified without any photoantenna, as many other (6-4) photolyase. By sequence alignments of OtCPF1 to different photolyases and cryptochromes in the region of photoantenna binding, we proposed that the most likely photoantenna OtCPF1 could bind *in vivo* would be 8-HDF. This proposal is supported by homology modeling and successful docking of 8-HDF. We concluded that the absence of 8-HDF after overexpression in *E. coli* might simply be explained by the fact that 8-HDF is not available in *E. coli*.

Acknowledgments

This work was supported by the ANR (French National Agency for Research) through the "Femtomotile" Project (ANR-05-BLAN-0188-01) and by the EU-FP6 Marine Genomics from the Network of Excellence (GOCE-CT-2004-505403).

Appendix A. Supplementary data

Supplementary data associated with this article can be found, in the online version, at doi:10.1016/j.jphotochem.2012.01.012.

References

[1] A. Sancar, Structure and function of DNA photolyase and cryptochrome blue-light photoreceptors, Chem. Rev. 103 (2003) 2203–2237.
[2] K. Brettel, M. Byrdin, Reaction mechanisms of DNA photolyase, Curr. Opin. Struct. Biol. 20 (2010) 693–701.
[3] S. Weber, C.W.M. Kay, H. Mogling, K. Mobius, K. Hitomi, T. Todo, Photoactivation of the flavin cofactor in *Xenopus laevis* (6-4) photolyase: observation of a transient tyrosyl radical by time-resolved electron paramagnetic resonance, Proc. Natl. Acad. Sci. U.S.A. 99 (2002) 1319–1322.
[4] A.R. Cashmore, Cryptochromes: enabling plants and animals to determine circadian time, Cell 114 (2003) 537–543.
[5] C.T. Lin, D. Shalitin, Cryptochrome structure and signal transduction, Annu. Rev. Plant Biol. 54 (2003) 469–496.
[6] C.T. Lin, T. Todo, The cryptochromes, Gen. Biol. 6 (2005).
[7] C.L. Partch, A. Sancar, Photochemistry and photobiology of cryptochrome blue-light photopigments: the search for a photocycle, Photochem. Photobiol. 81 (2005) 1291–1304.
[8] I. Chaves, R. Pokorny, M. Byrdin, N. Hoang, T. Ritz, K. Brettel, L.-O. Essen, G.T.J. van der Horst, A. Batschauer, M. Ahmad, The cryptochromes: blue light photoreceptors in plants and animals, Annu. Rev. Plant Biol. 62 (2011) 335–364.
[9] R. Pokorny, T. Klar, U. Hennecke, T. Carell, A. Batschauer, L.O. Essen, Recognition and repair of UV lesions in loop structures of duplex DNA by DASH-type cryptochrome, Proc. Natl. Acad. Sci. U.S.A. 105 (2008) 21023–21027.
[10] C.P. Selby, A. Sancar, A cryptochrome/photolyase class of enzymes with single-stranded DNA-specific photolyase activity, Proc. Natl. Acad. Sci. U.S.A. 103 (2006) 17696–17700.
[11] A.F. Glas, M.J. Maul, M. Cryle, T.R.M. Barends, S. Schneider, E. Kaya, I. Schlichting, T. Carell, The archaeal cofactor F_0 is a light-harvesting antenna chromophore in eukaryotes, Proc. Natl. Acad. Sci. U.S.A. 106 (2009) 11540–11545.
[12] R. Brudler, K. Hitomi, H. Daiyasu, H. Toh, K. Kucho, M. Ishiura, M. Kanehisa, V.A. Roberts, T. Todo, J.A. Tainer, E.D. Getzoff, Identification of a new cryptochrome class: structure, function, and evolution, Mol. Cell 11 (2003) 59–67.
[13] Y.H. Huang, R. Baxter, B.S. Smith, C.L. Partch, C.L. Colbert, J. Deisenhofer, Crystal structure of cryptochrome 3 from *Arabidopsis thaliana* and its implications for photolyase activity, Proc. Natl. Acad. Sci. U.S.A. 103 (2006) 17701–17706.
[14] H.W. Park, S.T. Kim, A. Sancar, J. Deisenhofer, Crystal structure of DNA photolyase from *Escherichia coli*, Science 268 (1995) 1866–1872.
[15] T. Tamada, K. Kitadokoro, Y. Higuchi, K. Inaka, A. Yasui, P.E. de Ruiter, A.P.M. Eker, K. Miki, Crystal structure of DNA photolyase from *Anacystis nidulans*, Nat. Struct. Biol. 4 (1997) 887–891.
[16] K. Hitomi, L. DiTacchio, A.S. Arvai, J. Yamamoto, S.T. Kim, T. Todo, J.A. Tainer, S. Iwai, S. Panda, E.D. Getzoff, Functional motifs in the (6-4) photolyase crystal structure make a comparative framework for DNA repair photolyases and clock cryptochromes, Proc. Natl. Acad. Sci. U.S.A. 106 (2009) 6962–6967.
[17] M.J. Maul, T.R.M. Barends, A.F. Glas, M.J. Cryle, T. Domratcheva, S. Schneider, I. Schlichting, T. Carell, Crystal structure and mechanism of a DNA (6-4) photolyase, Angew. Chem. Int. Ed. 47 (2008) 10076–10080.
[18] T. Todo, S.T. Kim, K. Hitomi, E. Otoshi, T. Inui, H. Morioka, H. Kobayashi, E. Ohtsuka, H. Toh, M. Ikenaga, Flavin adenine dinucleotide as a chromophore of the *Xenopus* (6-4) photolyase, Nucleic Acids Res. 25 (1997) 764–768.
[19] A. Usman, J. Brazard, M.M. Martin, P. Plaza, M. Heijde, G. Zabulon, C. Bowler, Spectroscopic characterization of a (6-4) photolyase isolated from the green alga *Ostreococcus tauri*, J. Photochem. Photobiol. B 96 (2009) 38–48.
[20] Y. Yi, Y. Cao, Q. Li, M. Liu, L. Cheng, L.H. Bai, Z.R. Yang, D.R. Qiao, Cloning and sequence analysis of the gene encoding (6-4) photolyase from *Dunaliella salina*, Biotechnol. Lett. 28 (2006) 309–314.
[21] M. Heijde, G. Zabulon, F. Corellou, T. Ishikawa, J. Brazard, A. Usman, F. Sanchez, P. Plaza, M. Martin, A. Falciatore, T. Todo, F.Y. Bouget, C. Bowler, Characterization of two members of the cryptochrome/photolyase family from *Ostreococcus tauri* provides insights into the origin and evolution of cryptochromes, Plant Cell Environ. 33 (2010) 1614–1626.
[22] J. Brazard, A. Usman, F. Lacombat, C. Ley, M.M. Martin, P. Plaza, L. Mony, M. Heijde, G. Zabulon, C. Bowler, Spectro-temporal characterization of the photoactivation mechanism of two new oxidized cryptochrome/photolyase photoreceptors, J. Am. Chem. Soc. 132 (2010) 4935–4945.
[23] S.T. Kim, P.F. Heelis, A. Sancar, Energy transfer (deazaflavin → $FADH_2$) and electron transfer ($FADH_2$ → T<>T) kinetics in *Anacystis nidulans* photolyase, Biochemistry 31 (1992) 11244–11248.
[24] S.T. Kim, P.F. Heelis, T. Okamura, Y. Hirata, N. Mataga, A. Sancar, Determination of rates and yields of interchromophore (folate → Flavin) energy transfer and intermolecular (Flavin → DNA) electron transfer in *Escherichia coli* photolyase by time-resolved fluorescence and absorption spectroscopy, Biochemistry 30 (1991) 11262–11270.
[25] C. Saxena, H.Y. Wang, I.H. Kavakli, A. Sancar, D.P. Zhong, Ultrafast dynamics of resonance energy transfer in cryptochrome, J. Am. Chem. Soc. 127 (2005) 7984–7985.
[26] A. Tyagi, A. Penzkofer, A. Batschauer, E. Wolf, Thermal degradation of (6R,S)-5,10-methenyltetrahydrofolate in aqueous solution at pH 8, Chem. Phys. 358 (2009) 132–136.
[27] J. Brazard, C. Ley, F. Lacombat, P. Plaza, M.M. Martin, G. Checcucci, F. Lenci, Primary photoprocesses involved in the sensory protein for the photophobic response of *Blepharisma japonicum*, J. Phys. Chem. B 112 (2008) 15182–15194.
[28] B. Rost, C. Sander, Prediction of protein secondary structure at better than 70% accuracy, J. Mol. Biol. 232 (1993) 584–599.
[29] A. Sali, T.L. Blundell, Comparative protein modeling by satisfaction of spatial restraints, J. Mol. Biol. 234 (1993) 779–815.
[30] G.S. Wu, D.H. Robertson, C.L. Brooks, M. Vieth, Detailed analysis of grid-based molecular docking: a case study of C-DOCKER—a CHARMm-based MD docking algorithm, J. Comput. Chem. 24 (2003) 1549–1562.
[31] R. Jimenez, G.R. Fleming, P.V. Kumar, M. Maroncelli, Femtosecond solvation dynamics of water, Nature 369 (1994) 471–473.
[32] M.S. Jorns, B.Y. Wang, S.P. Jordan, L.P. Chanderkar, Chromophore function and interaction in *Escherichia coli* DNA photolyase: reconstitution of the apoenzyme with pterin and or flavin derivatives, Biochemistry 29 (1990) 552–561.
[33] M. Enescu, L. Lindqvist, B. Soep, Excited-state dynamics of fully reduced flavins and flavoenzymes studied at subpicosecond time resolution, Photochem. Photobiol. 68 (1998) 150–156.
[34] Y.T. Kao, C. Saxena, T.F. He, L.J. Guo, L.J. Wang, A. Sancar, D.P. Zhong, Ultrafast dynamics of flavins in five redox states, J. Am. Chem. Soc. 130 (2008) 13132–13139.
[35] G.F. Li, V. Sichula, K.D. Glusac, Role of adenine in thymine dimer repair by reduced flavin adenine dinucleotide, J. Phys. Chem. B 112 (2008) 10758–10764.
[36] J. Brazard, A. Usman, F. Lacombat, C. Ley, M.M. Martin, P. Plaza, New insights into the ultrafast photophysics of oxidized and reduced FAD in solution, J. Phys. Chem. A 115 (2011) 3251–3262.
[37] R.-K. Zhao, A. Lukacs, A. Haigney, R. Brust, G.M. Greetham, M. Towrie, P.J. Tonge, S.R. Meech, Ultrafast transient mid IR to visible spectroscopy of fully reduced flavins, Phys. Chem. Chem. Phys. 13 (2011) 17642–17648.
[38] M.K. Kuimova, G. Yahioglu, J.A. Levitt, K. Suhling, Molecular rotor measures viscosity of live cells via fluorescence lifetime imaging, J. Am. Chem. Soc. 130 (2008) 6672–6673.
[39] M.M. Martin, P. Plaza, Y.H. Meyer, Transient spectroscopy of triphenylmethane derivatives following subpicosecond irradiation, Chem. Phys. 153 (1991) 297–303.
[40] Y.T. Kao, C. Tan, S.H. Song, N. Ozturk, J. Li, L.J. Wang, A. Sancar, D.P. Zhong, Ultrafast dynamics and anionic active states of the flavin cofactor in cryptochrome and photolyase, J. Am. Chem. Soc. 130 (2008) 7695–7701.
[41] C. Saxena, A. Sancar, D.P. Zhong, Femtosecond dynamics of DNA photolyase: energy transfer of antenna initiation and electron transfer of cofactor reduction, J. Phys. Chem. B 108 (2004) 18026–18033.
[42] S.E. Braslavsky, E. Fron, H.B. Rodriguez, E.S. Roman, G.D. Scholes, G. Schweitzer, B. Valeur, J. Wirz, Pitfalls and limitations in the practical use of Förster's theory of resonance energy transfer, Photochem. Photobiol. Sci. 7 (2008) 1444–1448.
[43] T. Förster, Energiewanderung und Fluoreszenz, Naturwissenschaften 6 (1946) 166–175.
[44] Y. Matsuoka, B. Norden, Linear dichroism studies of nucleic-acids. III. Reduced dichroism curves of DNA in ethanol–water and in poly(vinylalcohol) films, Biopolymers 22 (1983) 1731–1746.
[45] M. Salim, U. Siddiqui, G. Kodali, R.J. Stanley, Electronic transition dipole moment directions of reduced anionic flavin in stretched poly(vinylalcohol) films, J. Phys. Chem. B 112 (2008) 119–126.

[46] T. Okamura, A. Sancar, P.F. Heelis, T.P. Begley, Y. Hirata, N. Mataga, Picosecond laser photolysis studies on the photorepair of pyrimidine dimers by DNA photolyase. 1. Laser photolysis of photolyase-2-deoxyuridine dinucleotide photodimer complex, J. Am. Chem. Soc. 113 (1991) 3143–3145.
[47] T. Klar, R. Pokorny, J. Moldt, A. Batschauer, L.O. Essen, Cryptochrome 3 from *Arabidopsis thaliana*: structural and functional analysis of its complex with a folate light antenna, J. Mol. Biol. 366 (2007) 954–964.
[48] M. Takao, A. Oikawa, A.P.M. Eker, A. Yasui, Expression of an *Anacystis nidulans* photolyase gene in *Escherichia coli*: functional complementation and modified action spectrum of photoreactivation, Photochem. Photobiol. 50 (1989) 633–637.